Performance analysis of a Pt/n-GaN Schottky barrier UV detector

F. BOUZID[1,5], L. DEHIMI[1,2,3], and F. PEZZIMENTI[4]

1.—Laboratory of Metallic and Semiconductor Materials, University of Biskra, P.B.145, Biskra, 07000, Algeria. 2.—Thin Films Development and Applications Unit UDCMA, Setif / Research Center in Industrial Technologies CRTI, P.O. Box 64, Cheraga 16014, Algiers - Algeria. 3.—Faculty of Science, University of Batna, Batna, 05000, Algeria. 4.—DIIES, Mediterranea University of Reggio Calabria, Reggio Calabria 89122, Italy. 5.—e-mail: faycal.bouzid@ymail.com, Tel: +213 0665011376, Fax: +213 36620092.

In this paper the electrical and optical characteristics of a n-type gallium nitride (GaN) based Schottky barrier ultraviolet (UV) detector, where a platinum (Pt) metal layer forms the anode contact, are evaluated by means of detailed numerical simulations considering a wide range of incident light intensities. With this purpose, by modeling the GaN physical properties, the detector current-voltage characteristics and spectral responsivity for different bias voltages (forward and reverse) and temperatures are presented assuming an incident optical power ranging from 0.001 to 1 Wcm^{-2}. The effect of defect states in the GaN substrate is also investigated. The results show that, at room temperature, under a reverse bias voltage of -300 V, the dark current density is in the limit of 2.18×10^{-19} Acm^{-2}. After illumination, for a 0.36 μm UV uniform beam with an intensity of 1 Wcm^{-2}, the photocurrent significantly increases resulting 2.33 Acm^{-2} and the detector spectral responsivity attains a maximum value of 0.2 AW^{-1} at zero-bias voltage. Deep acceptor trap states and high temperature highly affect the spectral responsivity curve in the considered 0.2 - 0.4 μm UV spectrum.

Key words: Gallium nitride, Schottky barrier, ultraviolet detector, photocurrent, responsivity, temperature.

This is a post-peer-review, pre-copyedit version of an article published in Journal of Electronic Materials, n. 46, pp. 6563-6570, 2017. The final authenticated version is available online at: https://doi.org/10.1007/s11664-017-5696-1

INTRODUCTION

III-Nitrides are some of the most promising materials widely used in optoelectronics. Among these compounds, in particular, gallium nitride (GaN) appears as a wide bandgap semiconductor with the potential to offer great performance improvements in high-temperature and high-radiation-level environments, meeting requirements such as higher breakdown electric fields, carrier saturation velocities, thermal conductivity and ability to form high quality heterostructures with good transport properties [1-3].

In the past few years, GaN has been used for light emitting diodes [4], laser diodes [5], and a large number of structures well suited for α-particle [6,7], thermal neutron [8], electron and x-ray detection [9-12].

Recently, ultraviolet (UV) detection by means of GaN has motivated a great interest in many important fields which require high-performance solar-blind photodetectors with low dark current and high responsivity, such as spatial optical

communications, engine monitoring, missile plume detection, flame detection, biological and chemical agents detection, ozone layer monitoring, quantum information and quantum optics [13-16]. Different types of GaN UV detectors have been proposed based on p-n junction [17,18], p-i-n [19-21], metal-semiconductor-metal [22-24], hetero-junction [25,26] and Schottky barrier [27,28] structures. In particular, the advantage of Schottky barrier photodiodes compared with the others is in the more efficient absorption of UV light with shallow penetration depth, allowing the design of a thinner depletion region formed near the interface between the metal and the absorption layer.

In order to obtain GaN-based devices with a large Schottky barrier height, different metals can be used [29-33], e.g. palladium (Pd), nickel (Ni), gold (Au), titanium (Ti), chromium (Cr) and platinum (Pt). In particular, Pt has a high work function that makes it ideal for use as Schottky contact on n-type GaN substrates and it is also resistant to oxidation and corrosion [34].

In this paper, the electrical and optical characteristics of a thin Pt/n-GaN Schottky barrier UV detector are investigated by means of a careful simulation study carried out using the Silvaco-Atlas technology computer aided design (TCAD) simulator [35], and considering a 2-D device analysis which solves the Poisson's equation and the carrier continuity equations, with the electron and hole current densities given by the drift-diffusion model. The device current density-voltage characteristics under illumination for different UV-light intensities in the range 0.001-1 Wcm^{-2}, in both reverse and forward bias, and the spectral responsivity in the 0.2-0.4 μm wavelength spectrum, with its dependence on the temperature and reverse bias conditions, are presented. During the simulations, different anode thicknesses were considered. Moreover, assuming a finite defect state concentration located in the GaN substrate, the effect of different acceptor trap energy levels on the detector responsivity was also evaluated. In fact, a wide range of operating temperatures as well as the exposure to high levels of radiation strongly affect the performance of experimental detectors and often determine an alteration of the device detection properties. Energetic photons and particles transfer a part of their kinetic energy to gallium and nitrogen atoms and this energy displaces atoms from their lattice sites creating charged defect centers [36].

DEVICE STRUCTURE

The schematic cross-sectional view of the Pt/n-GaN thin Schottky detector proposed in this work is shown in Fig.1.

Starting from a GaN n^+ substrate with a doping concentration of 5×10^{19} cm^{-3}, a 5 μm-thick epitaxial layer with a donor doping level of 1×10^{16} cm^{-3} and a 1 nm-thick Pt metal layer which acts as the anode region are considered. Finally, an ohmic contact on the whole back surface is assumed (e.g. titanium-aluminum, TiAl). The device area is 12 μm^2.

The detector was designed in order to perform, in the dark, a theoretical breakdown voltage close to 1300 V at room temperature. Moreover, the thin epilayer aids to reduce the device internal serial resistance.

For the numerical analysis, the above described structure was finely meshed with a rectangular 2-D mesh and the metal/semiconductor and the n/n^+ interfaces were accurately refined.

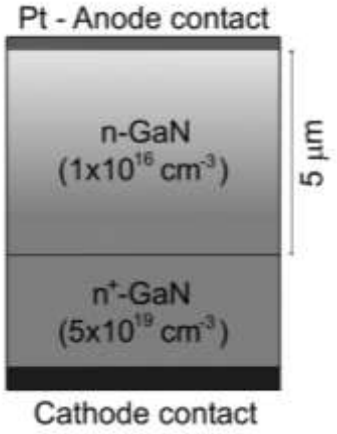

Fig. 1. Schematic cross section of the proposed Pt/n-GaN Schottky detector. Plot not in scale.

PHYSICAL MODELS

The key physical models used during the simulations include the optical photogeneration, the Shockley-Read-Hall (SRH) and Auger recombination processes, the incomplete doping activation, the impact ionization, the bandgap temperature dependence and the carrier mobility as a function of both doping and temperature.

The temperature dependence of the GaN bandgap energy [37] and intrinsic carrier concentration [38] are assumed in the forms:

$$E_g(T) = E_{g0} + 9.39\times10^{-4}\left(\frac{300^2}{300+772} - \frac{T^2}{T+772}\right) \quad (1)$$

$$n_i(T) = 1.98\times10^{16}\times T^{3/2}\exp\left(-\frac{20488}{T}\right) \quad (2)$$

where E_{g0} = 3.396 eV is the band-gap energy value at T = 300 K.

Starting from the effective intrinsic carrier concentration n_i, the Auger, SRH, and optical generation-recombination rates are modeled using the standard expressions [39]:

$$R_{Auger} = \left(C_p p + C_n n\right)\left(np - n_i^2\right) \quad (3)$$

$$R_{SRH} = \frac{pn - n_i^2}{\tau_p\left(n + n_i\exp\left(\frac{E_{trap}}{kT}\right)\right) + \tau_n\left(p + n_i\exp\left(-\frac{E_{trap}}{kT}\right)\right)} \quad (4)$$

$$R_{opt} = C_{opt}\left(np - n_i^2\right) \quad (5)$$

where C_{opt} = 1.1e^{-8} cm^{3}s^{-1}, C_n = 1×10^{-30} cm^{6}s^{-1} and C_p = 1×10^{-31} cm^{6}s^{-1} are model parameters, E_{trap} is the difference between the trap energy level and the intrinsic Fermi level, and τ_n, τ_p are the carrier lifetimes dependent upon the doping level as described by the Scharfetter's relation [39]:

$$\tau_{n,p} = \frac{\tau_{0n,p}}{1 + \left(\frac{N}{N_{n,p}^{SRH}} \right)^{\gamma_{n,p}}} \qquad (6)$$

Here, N is the local impurity concentration and $\tau_{0n,p}$ = 0.5 ns, $N_{n,p}^{SRH} = 5\times10^{16}$ cm^{-3} and $\gamma = 1$ are reference parameters [38].

The charge carrier photogeneration rate dependence on the incident beam wavelength is given by [35]:

$$G = \eta_0 \frac{P^* \lambda}{hc} \alpha e^{-\alpha y} \qquad (7)$$

where P^* contains the cumulative effects of reflections, transmissions, and losses due to absorption over the ray path; η_0 is the internal quantum efficiency which represents the number of carrier pairs generated per photon; y is a relative distance for the ray in question; h is the Planck's constant; λ is the wavelength; c is the speed of light; α is the absorption coefficient.

The electron and hole impact ionization rates, $\alpha_{n,p}$, which are defined as the number of electron-hole pairs generated by the carriers traveling a unit distance along the direction of the electric field, are modeled through the following empirical expression:

$$\alpha_{n,p} = a_{0n,p} \exp\left(-\frac{b_{0n,p}}{E} \right) \qquad (8)$$

being the coefficients a_0 and b_0 listed in Table I.

Table I. GaN impact ionization parameters [38].

Carrier	a_0 (cm^{-1})	b_0 (Vcm^{-1})
Electron	2.41×10^8	3.40×10^7
Hole	5.41×10^6	1.96×10^7

Assuming the Fermi-Dirac statistics, the incomplete ionization of impurities can be expressed by means of [40]:

$$N_d^+ = \frac{N_d}{1 + 2\left(\frac{N_d}{N_C} \right) \exp\left(\frac{\Delta E_d}{kT} \right)} \qquad (9)$$

$$N_a^- = \frac{N_a}{1 + 4\left(\frac{N_a}{N_V} \right) \exp\left(\frac{\Delta E_a}{kT} \right)} \qquad (10)$$

where ΔE_a and ΔE_d are the acceptor and donor energy levels, e.g. ΔE_d = 16 meV for silicon (Si) and ΔE_a = 175 meV for magnesium (Mg), N_d and N_a are the substitutional n-type and p-type doping concentrations, and N_C and N_V are the electron and hole density of states varying with temperature as given by [38]:

$$N_C(T) = 2.3\times10^{18} \left(\frac{T}{300} \right)^{3/2} \qquad (11)$$

$$N_V(T) = 4.6\times10^{19} \left(\frac{T}{300} \right)^{3/2} \qquad (12)$$

Finally, the Caughey-Thomas empirical equation is used to model the carrier mobilities [41]:

$$\mu_{n,p} = \mu_{\min_{n,p}} + \frac{\mu_{\max_{n,p}}\left(\frac{T}{300}\right)^{\alpha} - \mu_{\min_{n,p}}}{1+\left(\frac{T}{300}\right)^{\beta}\left(\frac{N_{tot}}{N_{ref}}\right)^{\gamma}} \qquad (13)$$

Here, N_{tot} represents the local concentration of the ionized impurities and $\mu_{minn,p}$, $\mu_{maxn,p}$, α, β and γ are the GaN specific model parameters summarized in Table II [42].

Table II. GaN carrier mobility parameters.

Carrier	μ_{max} (cm^2/Vs)	μ_{min} (cm^2/Vs)	N_{ref} (cm^{-3})	α	β	γ
Electron	1418	55	2×10^{17}	-2	-3.8	1
Hole	175	30	3×10^{17}	-5	-3.7	2

In addition, the Canali's model [43] is used to taken into account the high field-dependent mobility:

$$\mu_{n,p}(E) = \mu_{0n,p}\left[1+\left(E\frac{\mu_{0n,p}}{v_{sat}}\right)^{\kappa_{n,p}}\right]^{-1/\kappa_{n,p}} \qquad (14)$$

where $\mu_{0n,p}$ is the low electric field mobility and v_{sat} is the temperature-dependent saturation velocity given by:

$$v_{sat} = \frac{2.7\times10^{7}}{1+0.8\exp\left(\frac{T}{600}\right)} \qquad (15)$$

RESULTS AND DISCUSSION

Analysis of the light intensity effect

The simulated forward and reverse current density-voltage (*J-V*) characteristics of the presented Pt/n-GaN Schottky barrier UV detector, in dark and under a uniform UV-light at 0.36 μm for different illumination intensities, are shown in Fig. 2 and Fig. 3, respectively.

The device shows a good rectifying behavior in dark condition and, for example, a rectification ratio in the order of 10^{22} at ±2 V can be calculated at room temperature. Moreover, at T = 300 K and -300 V the reverse leakage current density is as low as 2.18×10^{-19} Acm^{-2} (see Fig. 3) and the breakdown occurs for a reverse bias voltage of 1330 V. These results confirm that the proposed detector could be well suitable for low noise applications.

From Fig. 2, it is also worthwhile noting that the forward current exponentially increases with the applied voltage, with no appreciable effect of the illumination. On the other hand, in Fig. 3 the reverse current increases with increasing the illumination intensity in a significant manner. For example, for a reverse bias of -300 V, a photocurrent of 5.8×10^{-4} Acm^{-2} is calculated at

1×10^{-3} Wcm^{-2}, increasing to 2.33 Acm^{-2} at 1 Wcm^{-2}. This is a consequence of the gradual increase of the photogeneration rate, as shown in Fig. 4.

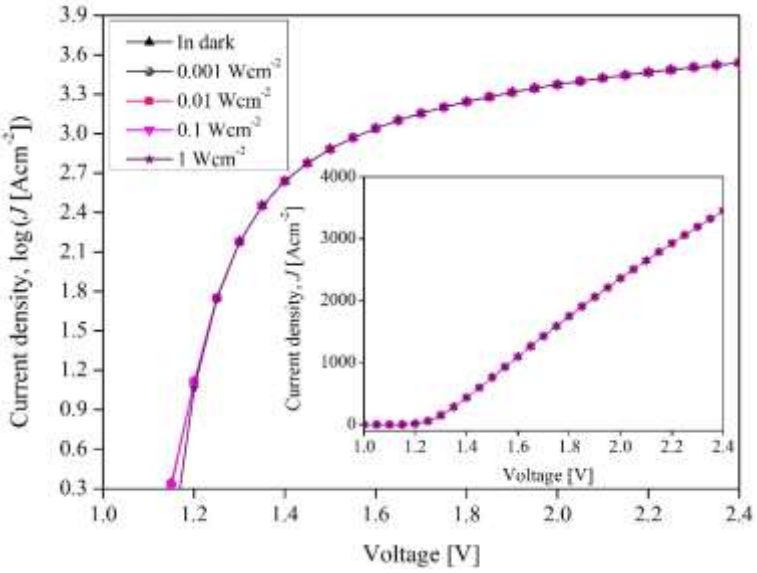

Fig. 2. Forward *J-V* characteristics of the Pt/n-GaN Schottky UV detector for different incident light intensities (λ = 0.36 μm) at T = 300 K. The inset shows the forward *J-V* characteristics in linear scale.

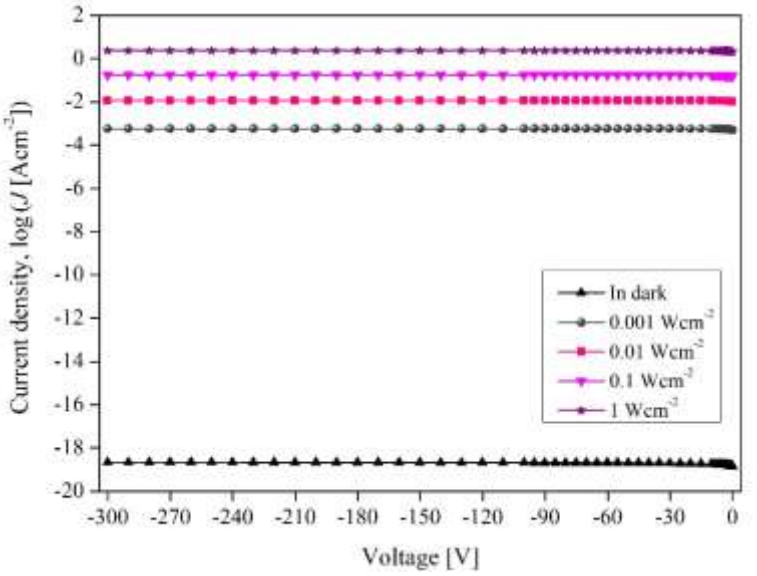

Fig. 3. Reverse *J-V* characteristics of the Pt/n-GaN Schottky UV detector for different incident light intensities (λ = 0.36 μm) at T = 300 K.

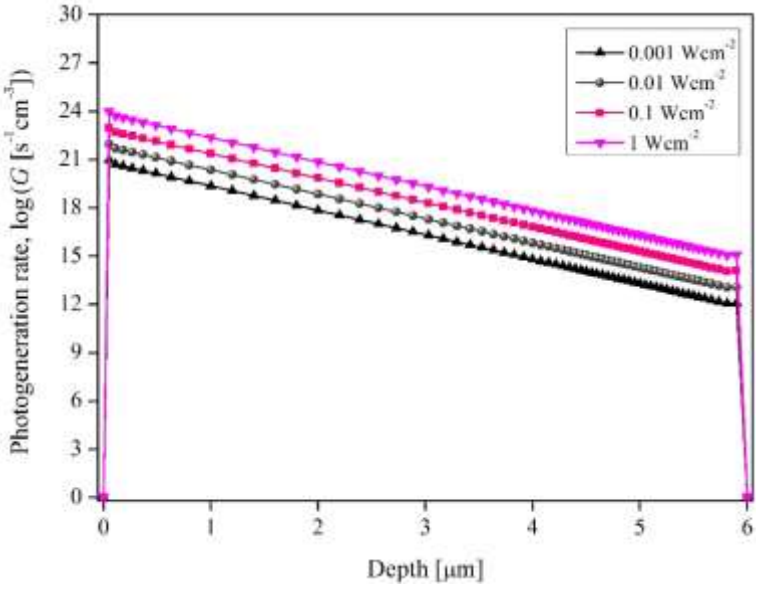

Fig. 4. Photogeneration rate profile across the detector for different incident light intensities (λ = 0.36 μm) at T = 300 K.

This is clearly shown Fig. 5 and Fig. 6, where the electron concentration profiles across the detector are plotted for several incident radiation intensities at a forward bias of 1.3 V, namely where a significant change of slope of the curves in Fig. 2 takes place, and at a reverse bias of -300 V, respectively. In particular, the electron concentration profile appears almost unchanged in Fig. 5 (forward bias), where it is mainly controlled by doping impurities and an increase of carriers only occurs in the depletion region. On the contrary, the electron concentration increases by several orders of magnitude within the whole epitaxial layer in Fig. 6 (reverse bias).

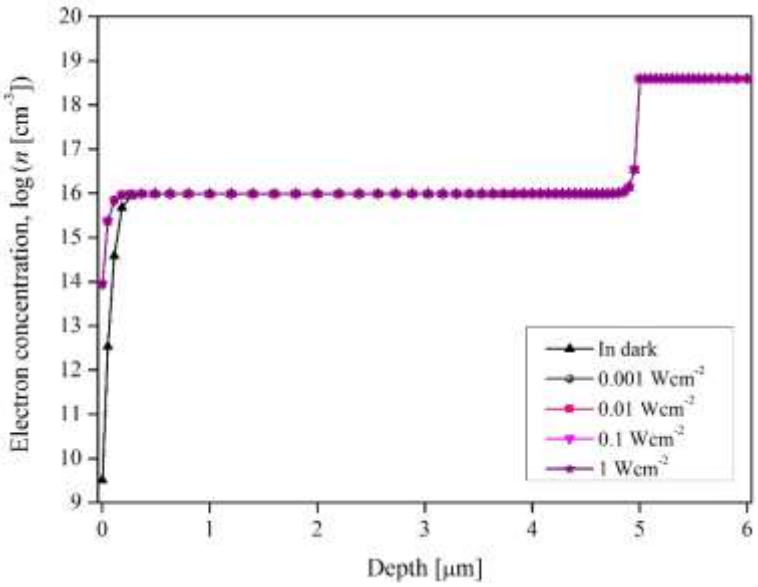

Fig. 5. Electron concentration profile across the detector under different incident light intensities (λ = 0.36 μm) for a forward bias of 1.3 V at T = 300 K.

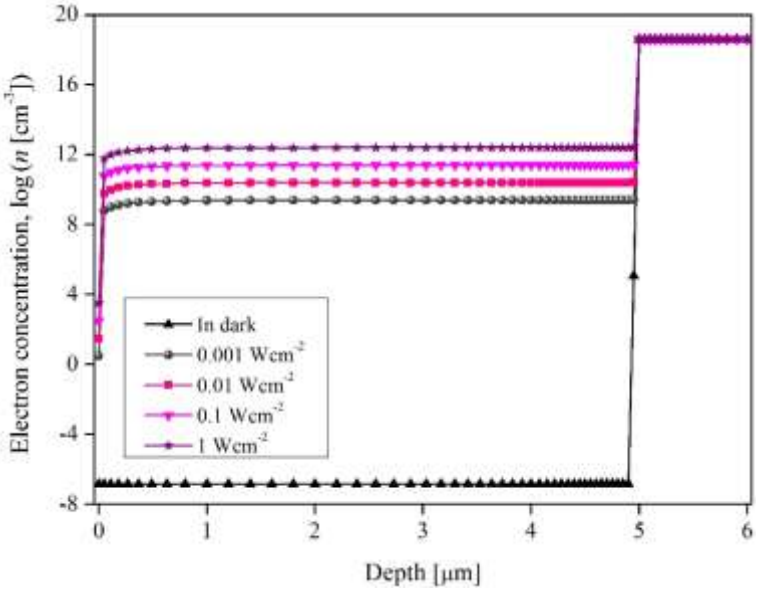

Fig. 6. Electron concentration profile across the detector under different incident light intensities (λ = 0.36 μm) for a reverse bias of -300 V at T = 300 K.

Finally, the concentration of holes, which represents the minority carriers, rises by several orders of magnitude for both forward and reverse biases, as shown in Fig. 7 and Fig. 8, respectively.

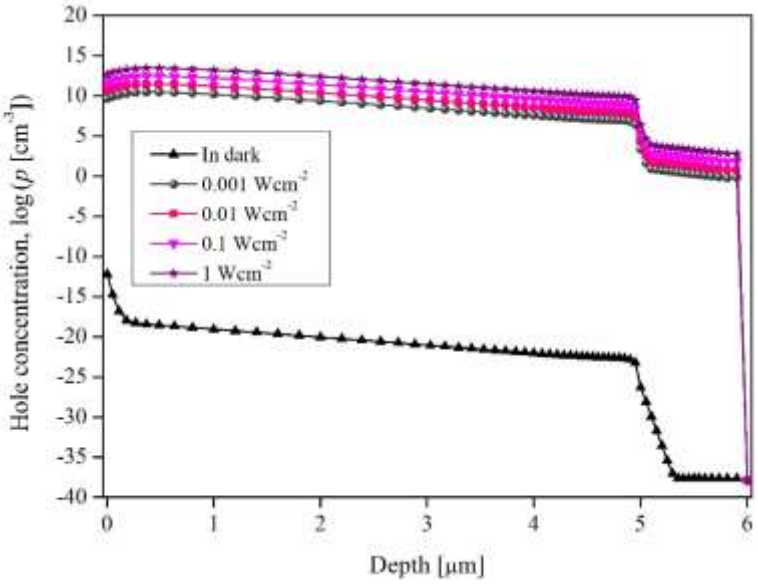

Fig. 7. Hole concentration profile across the detector under different incident light intensities (λ = 0.36 μm) for a forward bias of 1.3 V at T = 300 K.

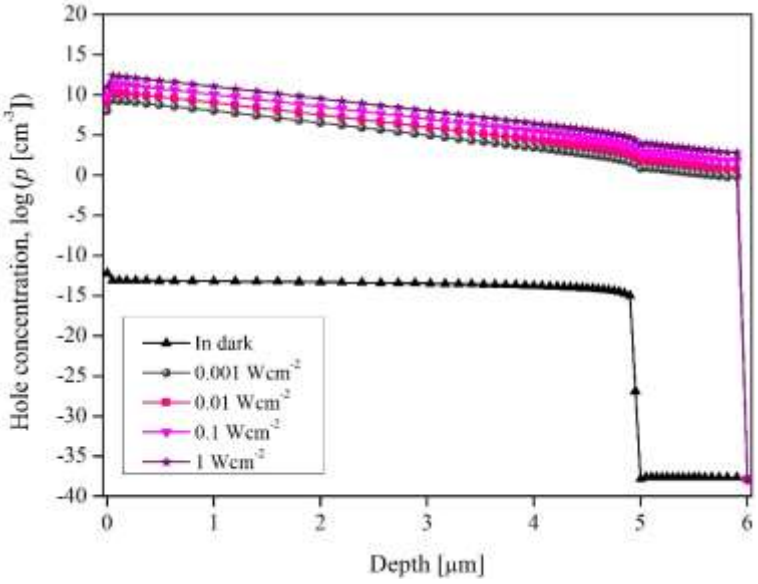

Fig. 8. Hole concentration profile across the detector under different incident light intensities (λ = 0.36 μm) for a reverse bias of -300 V at T = 300 K.

It is important to note that, as confirmed by simulations, the results presented in this paper can be considered valid for a device with an anode thickness in the limit of 10 nm. In fact, although in dark conditions anode metal thicknesses up to 100 nm have only a negligible effect on the detector *J-V* characteristics in both reverse and forward biases, under illumination thicknesses higher than 10 nm mark the set up of an appreciable decrease of the carrier photogeneration, as a result of the contact absorption. Furthermore, a Pt metal layer thicker than 10 nm determines a significant decrease of the detector spectral responsivity, as shown in Fig. 9 for an incident light intensity of 1 Wcm^{-2} at T = 300 K.

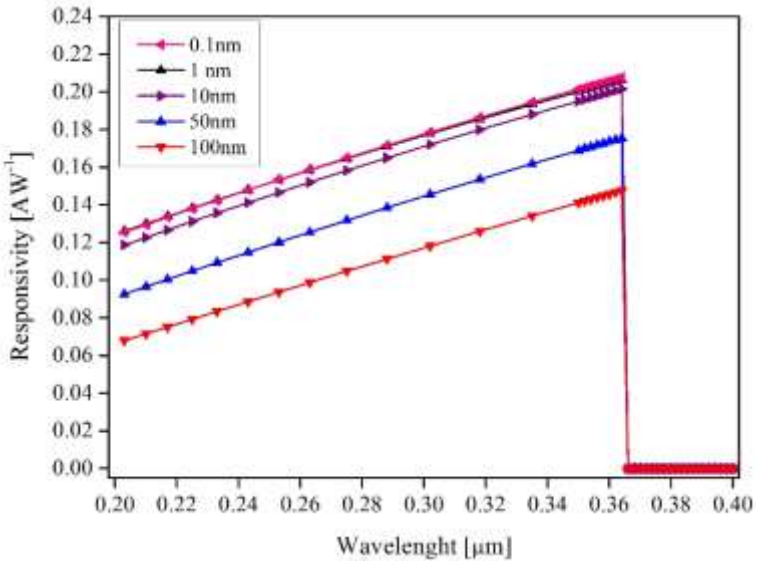

Fig. 9. Spectral responsivity of the Pt/n-GaN Schottky UV detector under a light intensity of 1 Wcm^{-2} and zero-bias voltage for different anode thicknesses.

As well known, the spectral responsivity of a photodiode is a measure of the effectiveness of the conversion of light power into electrical current and it is defined as the ratio of the photocurrent to the incident light power at a given wavelength.

Analysis of the temperature effect

By illuminating the Pt/n-GaN Schottky barrier UV detector in the 0.2 - 0.4 μm spectrum, with a light intensity of 1 Wcm^{-2}, the spectral responsivity curves as a function of temperature are shown in Fig. 10.

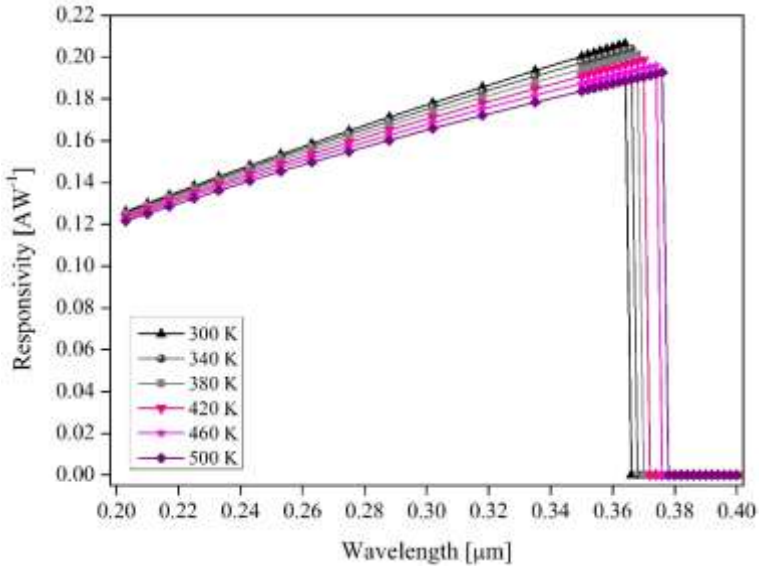

Fig. 10. Spectral responsivity of the Pt/n-GaN Schottky UV detector under a light intensity of 1 Wcm^{-2} and zero-bias voltage at six distinct temperatures.

Starting from the wavelength of 200 nm, in Fig. 10 the spectral responsivity rises gradually for longer wavelengths, from 0.126 AW^{-1} to 0.206 AW^{-1} at 0.364 μm (T = 300 K), due to the longer penetration depth. At 364 nm it drops sharply. In addition, we can note that, although the temperature has only a limited effect on the spectral responsivity for shorter wavelengths, because most of the corresponding photons is being absorbed, for increasing temperature the curves tend to shift towards the longer wavelengths and the peak of the responsivity is affected as well. It results, in fact, 0.192 AW^{-1} at T = 500 K, in correspondence of a cut-off wavelength of 0.376 μm.

The spectral responsivity behaviors shown in Fig. 10 can be explained by taking into account the temperature dependence of the GaN band-gap energy (1) and absorption coefficient. In particular, as can be seen in Fig. 11, the absorption coefficient undergoes a small increase with increasing temperatures and its threshold value shifts towards the longer wavelengths. In a similar manner, the cut-off wavelength shifts toward the longer wavelengths owing to its inverse relationship with the band-gap energy. On the other hand, the thermal agitation of the crystal lattice becomes more severe when the temperature increases, leading to a reduction of the carrier mobility, minority lifetime and diffusion length. Therefore, the recombination mechanism

becomes stronger and dominates the photogeneration phenomena, inducing a reduction of the spectral responsivity in the observed wavelength range before the cut-off occurs.

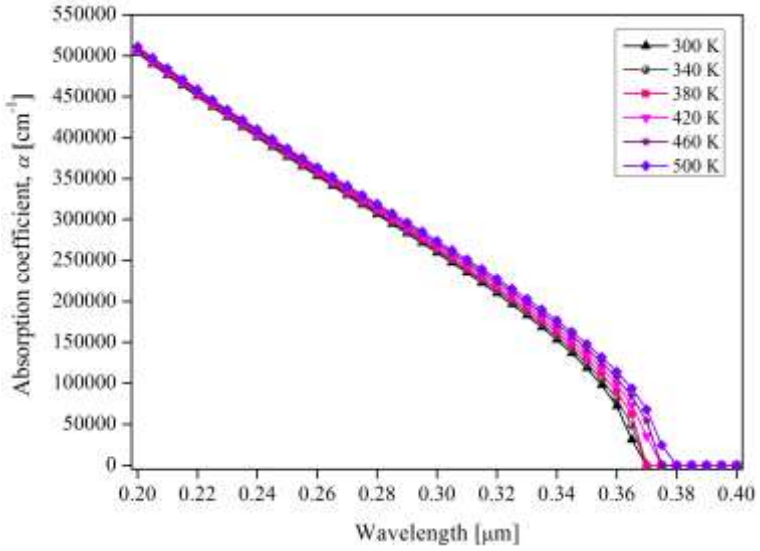

Fig. 11. Absorption coefficient of GaN at different temperatures.

Analysis of the reverse bias voltage effect

The spectral responsivity curves of the Pt/n-GaN Schottky barrier UV detector for an increasing reverse bias level at T = 300 K are shown in Fig. 12. The light intensity is fixed to 1 Wcm^{-2}.

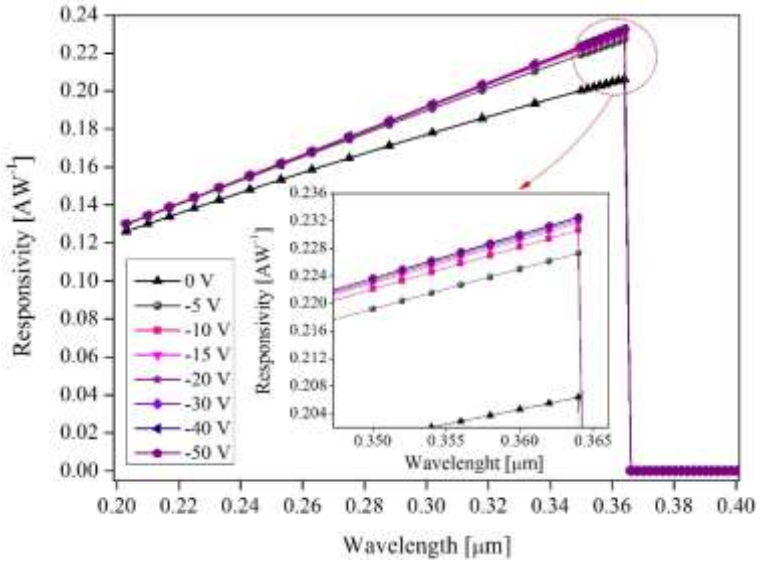

Fig. 12. Spectral responsivity of the Pt/n-GaN Schottky UV detector for different reverse bias voltages at T = 300 K. The inset shows a zoomed-in view of the spectral responsivity from 0.35- to 0.365-μm.

The peak of the spectral responsivity results 0.206 AW^{-1} at 0.364 μm under zero-bias voltage, as reported in Fig. 10. This value increases to 0.232 AW^{-1} for a reverse bias voltage of -50 V. The observed rise of the spectral responsivity with increase of

the reverse applied bias should be related to the enhancement of the charge collection efficiency. However, we can note that the responsivity curves become weakly dependent on the bias level for reverse voltages higher than about -30 V.

Analysis of an acceptor trap states effect

By illuminating the Pt/n-GaN Schottky barrier UV detector in the 0.2 - 0.4 μm spectrum with a light intensity of 1 Wcm^{-2} at zero-bias voltage and T = 300 K, the spectral responsivity curves for three common trap energy levels in GaN, labelled as H1, H2 and H5, are shown in Fig. 13. In literature, in fact, by using different experimental methods, these trap levels have been identified and assigned both to gallium vacancies and carbon-related defects which originate when carbon atoms substitute gallium and/or nitrogen atoms during the typical GaN growth processes [44-48]. More in detail, assuming a trap concentration in the limit of 1×10^{16} cm^{-3}, we have simulated the detector spectral responsivity considering the shallow trap level H2, which is located at 0.25 eV from the valence band edge Ev (i.e. Ev + 0.25 eV), at first, then the less deep trap level H1 (Ev + 0.87 eV), and finally the deep trap level H5 (Ev + 1.76 eV). The trap parameters used during the simulations were taken from literature [44] and summarized in Table III.

Table III. Trap simulation parameters.

Trap level	Activation energy (eV)	Density (cm^{-3})	Electron capture cross section (cm^2)	Hole capture cross section (cm^2)
H2	0.25	1×10^{16}	1.7×10^{-17}	1.7×10^{-16}
H1	0.87	1×10^{16}	7.4×10^{-14}	7.4×10^{-13}
H5	1.76	1×10^{16}	1.2×10^{-12}	1.2×10^{-11}

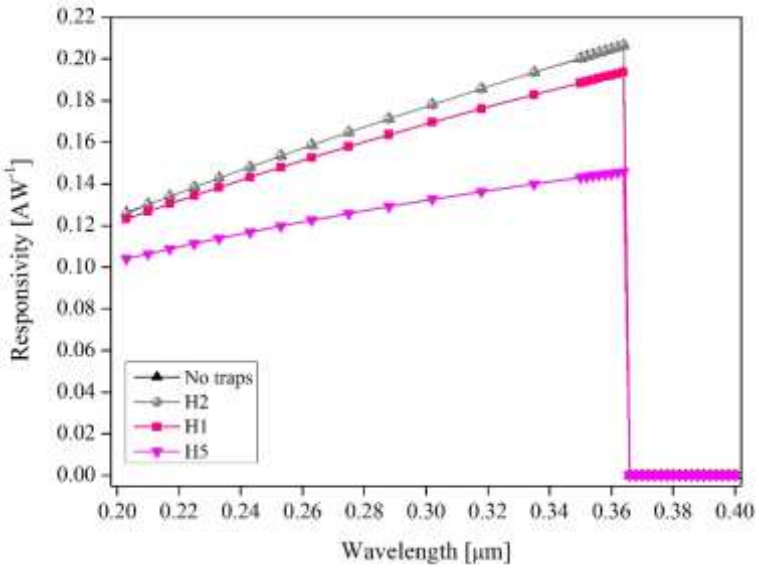

Fig. 13. Spectral responsivity of the Pt/n-GaN Schottky UV detector under a light intensity of 1 Wcm^{-2} and zero-bias voltage for different trap energy levels with a trap concentration of 1×10^{16} cm^{-3}.

The curves in Fig. 13 show that, at the assumed trap density, the shallow level H2 does not affect the spectral responsivity behavior and, in fact, the responsivity maximum value is once again 0.206 AW^{-1} at 0.364 μm. On the other hand, the spectral responsivity undergoes a reduction for all wavelengths, before the cut-off occurs, when the deepest levels are considered. In particular, the responsivity peak reaches 0.193 AW^{-1} and 0.146 AW^{-1} at 0.364 μm for H1 and H5, respectively. The observed decrement of the spectral responsivity, as soon as the trap level becomes deeper, is mainly due to a decrease of the minority carrier density. Therefore, in this case, the trap concentration must be minimized respect to the active doping profiles across the device structure.

CONCLUSION

In this paper, an electrical and optical analysis of a Pt/n-GaN Schottky barrier UV detector has been presented. From the simulations, the dark current density results extremely low under reverse bias voltages. On the other hand, by illuminating the detector with 0.36 μm UV light with different intensities, we have shown that the photocurrent density increases by several orders of magnitude, which confirms the usefulness of the Pt/n-GaN thin Schottky barrier for UV detection.

Assuming a light beam intensity of 1 Wcm^{-2} at zero-bias voltage and $T = 300$ K, the detector responsivity attains a peak value of 0.2 AW^{-1} in correspondence with a wavelength of 0.364 μm. This value increases to 0.23 AW^{-1} for a reverse bias voltage of -50 V. Also, as soon as the temperature increases, the spectral responsivity undergoes a reduction and the cut-off wavelength shifts towards the longer wavelengths. Such a behavior has been related to the temperature dependence of the GaN band-gap energy and absorption coefficient.

Finally, it was found that, although a shallow acceptor trap energy level does not affect the spectral responsivity curve, a significant reduction in the calculated responsivity values is observed in the whole explored 0.2 - 0.4 μm UV spectrum when the deepest trap levels are considered.

ACKNOWLEDGEMENT

The authors wish to thank Prof. Francesco G. Della Corte from DIIES - Mediterranean University of Reggio Calabria - Italy, for his comments that greatly improved the work.

REFERENCES

[1] G. Wang, K. Fu, C. S. Yao, D. Su, G. G. Zhang, J. Y. Wang, and M. Lu, Nucl. Instrum. Methods A 663, 10 (2012).

[2] M. S. P. Reddy, A. A. Kumar, and V. R. Reddy, Thin Solid Films 519, 3844 (2011).

[3] I. H. Lee, A. Y. Polyakov, N. B. Smirnov, A. V. Govorkov, E. A. Kozhukhova, V. M. Zaletin, I. M. Gazizov, N. G. Kolin, and S. J. Pearton, J. Vac. Sci. Technol. B 30, 021205 (2012).

[4] L. C. Chen, C. Y. Hsu, W. H. Lan, and S. Y. Teng, Solid-State Electron. 47, 1843 (2003).

[5] R. Werner, M. Reinhardt, M. Emmerling, A. Forchel, V. Harle, and A. Bazhenov, Physica E 7, 915 (2000).

[6] A. Y. Polyakov, N. B. Smirnov, A. V. Govorkov, A. V. Markov, E. A. Kozhukhova, I. M. Gazizov, N. G. Kolin, D. I. Merkurisov, V. M. Boiko, A. V. Korulin, V. M. Zalyetin, S. J. Pearton, I. H. Lee, A. M. Dabiran, and P. P. Chow, J. Appl. Phys. 106, 103708 (2009).

[7] G. Wang, K. Fu, C. S. Yao, D. Su, G. G. Zhang, J. Y. Wang, and M. Lu, Nucl. Instrum. Methods A 663, 10 (2012).

[8] P. Mulligan, J. Wang, L. Cao, Nucl. Instrum. Methods in Phys. Res. (A) Vol. 719 (2013) 13–16.

[9] F. H. Li, X. Gao, Y. L. Yuan, J. S. Yuan, and M. Lu, Sci. China: Technol. Sci. 57, 25 (2014).

[10] Z. J. Cheng, X. Y. Chen, H. S. San, Z. H. Feng, and B. Liu, J. Micromech. Microeng. 22, 074011 (2012).

[11] C. S. Yao, K. Fu, G. Wang, G. H. Yu, and M. Lu, Phys. Status Solidi A 209, 204 (2012).

[12] J. Y. Duboz, E. Frayssinet, S. Chenot, J. L. Reverchon, and M. Idir, Appl. Phys. Lett. 97, 163504 (2010).

[13] Y. Q. Yu, L. B. Luo, M. Z. Wang, B. Wang, L. H. Zeng, C. Y. Wu, J. S. Jie, J. W. Liu, L. Wang, and S. H. Yu, Nano Res. 8, 1098 (2015).

[14] J. Li, M. Zhao , and X. F. Wang, Physica B 405, 996 (2010).

[15] E. Ozbay, N. Biyikli, I. Kimukin, T. Kartaloglu, T. Tut, and O. Aytür, IEEE J. Sel. Top. Quantum Electron. 10, 742 (2004).

[16] Q. Chen, J. W. Yang, A. Osinsky, S. Gangopadhyay, B. Lim, M. Z. Anwar, and M. Asif Khan, Appl. Phys. Lett.70, 2277 (1997).

[17] P. Mulligan, J. Wang, and L. Cao, Nucl. Instrum. Methods A 719, 13 (2013).

[18] Q. Chen, M. A. Khan, C. J. Sun, and J. W. Yang, Electron. Lett. 31, 1781 (1995).

[19] G. Parish, S. Keller, P. Kozodoy, J. P. Ibbetson, H. Marchand, P. T. Fini, S. B. Fleischer, S. P. Den Baars, U. K. Mishra, and E. J. Tarsa, Appl. Phys. Lett. 75, 247 (1999).

[20] A. Hirano, C. Pernot, M. Iwaya, T. Detchprohm, H. Amano, and I. Akasaki, Phys. Status Solidi A 188, 293 (2001).

[21] E. Monroy, M. Hamilton, D. Walker, P. Kung, F. J. Sánchez, and M. Razeghi, Appl. Phys. Lett. 74, 1171 (1999).

[22] C. K. Wang, Y. Z. Chiou, S. J. Chang, W. Chih Lai, S. P. Chang, C. H. Yen, and C. C. Hung, IEEE Sens. J. 15, 4743 (2015).

[23] W. Jun , Z. Degang, L. Zongshun, F. Gan, Z. Jianjun, S. Xiaomin, Z. Baoshun and Y. Hui, Sci. China: Phys. Mech. 46, 198 (2003).

[24] D. Walker, E. Monroy, P. Kung, J. Wu, M. Hamilton, F. J. Sanchez, J. Diaz, and M. Razeghi, Appl. Phys. Lett. 74, 762 (1999).

[25] W. Yang, T. Nohova, S. Krishnankutty, R. Torreano, S. McPherson, and H. Marsh, Appl. Phys. Lett. 73, 1086 (1998).

[26] S. K. Zhang, W. B. Wang, I. Shtau, F. Yun, L. He, H. Morkoç, X. Zhou, M. Tamargo, and R. R. Alfano, Appl. Phys. Lett. 81, 4862 (2002).

[27] M. A. Khan, J. N. Kuznia, D. T. Olson, M. Blasingame, and A. R. Bhattarai, Appl. Phys. Lett. 63, 2455 (1993).

[28] A. Osinsky, S. Gangopadhyay, J. W. Yang, R. Gaska, D. Kuksenkov, H. Temkin, I. K. Shmagin, Y. C. Chang, J. F. Muth, and R. M. Kolbas, Appl. Phys. Lett. 72, 551 (1998).

[29] A. C. Schmitz, A. T. Ping, M. Asif Khan, Q. Chen, J. W. Yang, and I. Adesida, Semicond. Sci. Technol. 11, 1464 (1996).

[30] L. Wang, M. I. Nathan, T.H. Lim, M. A. Khan, and Q. Chen, Appl. Phys. Lett. 68, 1267 (1996).

[31] Y. Kribes, I. Harrison, B. Tuck, T. S. Cheng, and C. T. Foxon, Semicond. Sci. Technol. 12, 913 (1997).

[32] J. D. Guo, F. M. Pan, M. S. Feng, R. J. Guo, P. F. Chow, and C. Y. Chang, J. Appl. Phys. 80, 1623 (1996).

[33] E. V. Kalinina, N. J. Kurnestov, V. A. Dmitreiev, K. G. Irvine, and C. H. Carter, J. Electron. Mater. 25, 831 (1996).

[34] H. Morkoç, Handbook of Nitrides Semiconductors and Devices, (Wiley, Weinheim, 2008).

[35] Silvaco Atlas User's Manual, Device Simulator Software, 2013.

[36] L. Ling, J. G. Ma, Y. R. Cao, J. C. Zhang, W. Zhang, L. Li, S. R. Xu, X. H. Ma, X. T. Ren, and Y. Hao, Microelectron. Reliab. 51, 2168 (2011).

[37] H. Teisseyre, P. Perlin, T. Suski, I. Grzegory, and S. Porowski, J. Jun, J. Appl. Phys. 76, 2429 (1994).

[38] K. H. Baik, Y. Irokawa, F. Ren, S. J. Pearton, and S. S. Park, Solid-State Electron. 47, 1533 (2003).

[39] S. J. Pearton, C. R. Abernathy, and F. Ren, Gallium Nitride Processing for Electronics, Sensors and Spintronics, (Springer-Verlag, 2006).

[40] M. Razeghi and M. Henini, Optoelectronic Devices: III-Nitrides, (Elsevier, 2004).

[41] D. Caughey and R. Thomas, Proc. IEEE 52, 2192 (1967).

[42] T. T. Mnatsakanov, M. E. Levinshtein, L. I. Pomortseva, S. N. Yurkov, G. S. Simin, and M. A. Khan, Solid-State Electron. 47, 111 (2003).

[43] C. Canali, G. Majni, R. Minder, and G. Ottaviani, IEEE Trans. Electron Devices 22, 1045 (1975).

[44] Y. Tokuda, in *CS MANTECH Conference* (2014), pp. 19-24.

[45] A. Hierro, D. Kwon, S. A. Ringel, M. Hansen, J. S. Speck, U. K. Mishra, and S. P. DenBaars, Appl. Phys. Lett. 76, 3064 (2000).

[46] A. Armstrong, A. R. Arehart, B. Moran, S. P. DenBaars, U. K. Mishra, J. S. Speck, and S. A. Ringel, Appl. Phys. Lett. 84, 374 (2004).

[47] U. Honda, Y. Yamada, Y. Tokuda, and K. Shiojima, Jpn. J. Appl. Phys. 51,04DF04 (2012).

[48] M. Matsubara and E. Bellotti, arXiv:1507.06969 (2015).